Biochimica et Biophysica Acta 1828 (2013) 2064–2073

Contents lists available at SciVerse ScienceDirect

Biochimica et Biophysica Acta

journal homepage: www.elsevier.com/locate/bbamem

Surfactins modulate the lateral organization of fluorescent membrane polar lipids: A new tool to study drug:membrane interaction and assessment of the role of cholesterol and drug acyl chain length

L. D'Auria [a], M. Deleu [b], S. Dufour [b], M.-P. Mingeot-Leclercq [c], D. Tyteca [a,*]

[a] CELL Unit, de Duve Institute and Université Catholique de Louvain, UCL B1.75.05, Avenue Hippocrate, 75, B-1200 Brussels, Belgium
[b] Centre de Biophysique Moléculaire Numérique, Gembloux Agro-Bio Tech, Université de Liège, Gembloux, Belgium
[c] Cellular and Molecular Pharmacology, Louvain Drug Research Institute, Université Catholique de Louvain, Brussels, Belgium

ARTICLE INFO

Article history:
Received 27 February 2013
Received in revised form 16 April 2013
Accepted 8 May 2013
Available online 17 May 2013

Keywords:
Surfactin:membrane interaction
Micrometric lipid domain
Living erythrocyte
Vital confocal imaging
Cholesterol
BODIPY-lipid

ABSTRACT

The lipopeptide surfactin exhibits promising antimicrobial activities which are hampered by haemolytic toxicity. Rational design of new surfactin molecules, based on a better understanding of membrane:surfactin interaction, is thus crucial. We here performed bioimaging of lateral membrane lipid heterogeneity in adherent living human red blood cells (RBCs), as a new relevant bioassay, and explored its potential to better understand membrane:surfactin interactions. RBCs show (sub)micrometric membrane domains upon insertion of BODIPY (*) analogs of glucosylceramide (GlcCer*), sphingomyelin (SM*) and phosphatidylcholine (PC*). These domains exhibit increasing sensitivity to cholesterol depletion by methyl-β-cyclodextrin. At concentrations well below critical micellar concentration, natural cyclic surfactin increased the formation of PC* and SM*, but not GlcCer*, domains, suggesting preferential interaction with lipid* assemblies with the highest vulnerability to methyl-β-cyclodextrin. Surfactin not only reversed disappearance of SM* domains upon cholesterol depletion but further increased PC* domain abundance over control RBCs, indicating that surfactin can substitute cholesterol to promote micrometric domains. Surfactin sensitized excimer formation from PC* and SM* domains, suggesting increased lipid* recruitment and/or diffusion within domains. Comparison of surfactin congeners differing by geometry, charge and acyl chain length indicated a strong dependence on acyl chain length. Thus, bioimaging of micrometric lipid* domains is a visual powerful tool, revealing that intrinsic lipid* domain organization, cholesterol abundance and drug acyl chain length are key parameters for membrane:surfactin interaction. Implications for surfactin preferential location in domains or at their boundaries are discussed and may be useful for rational design of better surfactin molecules.

1. Introduction

Decades of world-wide antibiotic use have led to an increased bacterial resistance which urges to find new agents. Biological properties of surfactin, a lipopeptide produced by *Bacillus subtilis*, suggest it could be a potential antibacterial agent. Natural surfactin (hereafter referred to as "surfactin") is composed of an heptapeptide cycle closed by a C_{13} to C_{15} hydroxy fatty acid forming a lactone ring, with strong amphiphilic character explaining bioactivity as surfactant. Surfactin exhibits additional biological properties, including antibacterial, antiviral and hemolytic activities [for a review, see 1]. Surfactin's biological activity is determined by an interaction with membranes, including insertion into lipid bilayers, modification of permeability and membrane solubilization by a detergent-like mechanism [2]. This interaction is highly dependent on surfactin concentration, as demonstrated in model membranes with coexisting fluid disordered and gel phases [3]. To prevent hemolysis, a major limitation to medical applications, Dufour and collaborators have synthesized various linear surfactin analogs differing by charge and hydrophobicity (for structures, see Suppl. Fig. 1). In comparison to cyclic congeners, linear surfactins showed reduced surface activity and hemolysis [4].

So far, membrane:surfactin interactions have been mainly studied in elementary artificial model systems made of one or two phospholipids, thus ignoring major membrane components such as cholesterol and sphingolipids (SLs), as well as membrane lateral heterogeneity. SLs include the zwitterionic sphingomyelin (SM), which bears the

Abbreviations: BODIPY, boron dipyromethene, referred here as *; DF-BSA, defatted bovine serum albumin; DOPC, 1,2-dioleoyl-*sn*-glycero-3-phosphocholine; DPPC, 1,2-dipalmitoyl-*sn*-glycero-3-phosphocholine; FRAP, fluorescence recovery after photobleaching; GlcCer, glucosylceramide; GSL, glycosphingolipid; L_d, liquid-disordered; L_o, liquid-ordered; mβCD, methyl-β-cyclodextrin; PC, phosphatidylcholine; PLK, poly-L-lysine; PM, plasma membrane; RBC, red blood cell; S_o, solid-ordered; SAL14, *S*urfactin *A*cylated *L*inear with *14C*; SL, sphingolipid; SM, sphingomyelin; SNC14, *S*urfactin *N*atural *C*yclic with *14C*-acyl chain length; SSL10, *S*urfactin *S*ynthetic *L*inear with *10C*; SSL14, *S*urfactin *S*ynthetic *L*inear with *14C*; SSL18, *S*urfactin *S*ynthetic *L*inear with *18C*; surfactin-C_{13}–C_{15}, natural cyclic surfactin, referred here as surfactin

* Corresponding author. Tel.: +32 2 764 75 91; fax: +32 2 764 75 43.
E-mail address: donatienne.tyteca@uclouvain.be (D. Tyteca).

0005-2736/$ – see front matter © 2013 Elsevier B.V. All rights reserved.
http://dx.doi.org/10.1016/j.bbamem.2013.05.006

same phosphocholine headgroup as phosphatidylcholine (PC), and glycosphingolipids (GSLs), a heterogeneous family comprising mono (e.g. glucosylceramide; GlcCer), di (e.g. lactosylceramide) and more complex GSLs such as ganglioside GM1 [for a review, see 5]. Membrane lipid bilayers, long viewed as homogenous solvent for membrane proteins [6], actually show lateral heterogeneity at two different scales: transient nanometric rafts [7–11] vs more stable (sub)micrometric/mesoscale domains. Such domains have not only been evidenced on artificial vesicles [8,12–17] but also documented on living cells. They were initially predicted by FRAP [18]; further implied by single-molecule tracking based on discrete jumps between "mesoscale" domains [19–21]; and directly visualized by confocal imaging after insertion of fluorescent analogs at trace levels in various cells, including red blood cells (RBCs) [22–27]. Yeast plasma membrane (PM) proteins also show a patchwork of distinct micrometric domains [28–31].

Since antibacterial potential of surfactin is hampered by intrinsic hemolytic properties which are influenced by drug interaction with the bilayer, we here performed bioimaging of lateral membrane lipid heterogeneity in adherent human red blood cells (RBCs), as a new relevant bioassay, and explored its potential to better understand membrane:surfactin interactions. RBCs show micrometric domains readily evidenced by confocal microscopy upon insertion of trace levels of fluorescent analogs (BODIPY, *) of major polar lipids [22,26,27]. We thus probed the effect of various natural and synthetic surfactins on membrane organization using lipid* domains as read-out: (i) cyclic natural surfactin (referred to as surfactin-C_{13}–C_{15} or surfactin), bearing 13, 14 and 15C acyl chains; (ii) the purified natural SNC14 (*S*urfactin *N*atural *C*yclic with *14*C-acyl chain length); as well as (iii) synthetic linear analogs differing by charge and hydrophobicity, SAL14 (*S*urfactin *A*cylated *L*inear with *14*C-acyl chain length) and three SSLs with increased acyl chain lengths (SSL10, 14 and 18, *S*urfactins *S*ynthetic *L*inear with *10*, *14* or *18*C).

RBCs offer several advantages as experimental system. First, they allow studying lipid lateral organization without artifacts: (i) they are featureless at the micrometric level; (ii) they do not perform endocytosis nor lipid metabolism; (iii) their membrane asymmetry is well-characterized [32], including the occurrence of rafts [33–35]. Second, RBCs have a uniquely high content of cholesterol (~40 mol% vs ~30 mol% in fibroblasts vs ~15 mol% in blood platelets), which is a key regulator of both membrane fluidity via lipid packing and membrane deformability via modulation of PM protein interactions at the cortical cytoskeleton interface [36]. RBCs also exhibit a strong membrane:cytoskeleton anchorage, thanks to two non-redundant 4.1R and ankyrin-based complexes [37]. Third, RBCs have been used to evaluate surfactin toxicity [4]. Fourth, we recently reported in details by vital confocal imaging segregation of BODIPY analogs of GSLs* (e.g. GlcCer*), SM* and PC* into structurally distinct micrometric domains in RBCs [22,26,27]. We observed that all GSLs*, SM* and PC* domains disappear upon RBC stretching, indicating a control by membrane tension. However, domains are differentially modulated by: (i) temperature (peaking at 20 °C for SM* and PC* while steadily increasing up to 37 °C for GlcCer*); (ii) cholesterol (suppression of SM* and PC* domains by minor cholesterol depletion but preservation of GlcCer* domains); and (iii) the two membrane:cytoskeleton anchorage complexes (differential association with 4.1R complexes upon antibody patching and differential response to uncoupling at 4.1R and ankyrin complexes). The relevance of BODIPY-lipid micrometric domains for endogenous lipids despite BODIPY substitution of acyl chain is supported by three observations: (i) co-localization of exogenous GM1* with endogenous GM1 labeled by cholera toxin in RBCs; (ii) identity of PM domains in CHO cells upon direct insertion of SM* vs metabolic conversion of ceramide* into SM*; and (iii) selective disappearance of SM* domains upon depletion of endogenous SM [22,26,27].

We found that interaction of surfactins with RBC membrane, as reflected by impact on fluorescent micrometric lipid domains, is dictated by endogenous cholesterol content, lipid* domain organization and surfactin acyl chain length. Implications for preferential surfactin interaction with membranes of specific lipid composition and lateral heterogeneity are discussed. This straightforward confocal imaging assay may help understanding surfactin surface activity and designing less toxic surfactin derivatives.

2. Materials and methods

2.1. RBC isolation and immobilization

This study was approved by the Medical Ethics Institutional Committee and the blood donors gave written informed consent. RBCs were isolated from healthy volunteers. Blood was collected by venopuncture into dry EDTA (K^+ salt)-coated tubes, diluted 1:10 in medium (DMEM containing 25 mM glucose and 25 mM HEPES) and washed twice by centrifugation at 133 *g* for 2 min and resuspension. For spreading onto poly-L-lysine-coated coverslips, RBCs were plated at ~20.10^6 cells/ml onto 2-cm^2 coverslips precoated with 0.1 mg/ml 70–150 kDa poly-L-lysine (PLK; Sigma) at 20 °C for exactly 4 min after which the suspension was removed and replaced by fresh medium, in which RBCs were allowed to spread for another 4 min.

2.2. RBC treatments

Surfactin-C_{13}–C_{15} (a natural mixture of 13, 14 and 15C-acyl chain lengths, in proportion 3:42:52) and SNC14 (for *S*urfactin *N*atural *C*yclic with *14*C) were extracted from a *B. subtilis S499* culture supernatant. Synthetic surfactins, SAL14 (*S*urfactin *A*cylated *L*inear with *14*C) as well as SSL10, SSL14 and SSL18 (*S*urfactin *S*ynthetic *L*inear with *10*, *14* and *18*C in the acyl chain respectively), were prepared as described [4]. Unless otherwise stated, RBCs were preincubated in suspension with 0–1 μM surfactins at 37 °C for 30 min, before spreading onto poly-L-lysine-coated coverslips. For cholesterol depletion, cells were preincubated with 0.25 mM methyl-β-cyclodextrin (mβCD; Sigma) at 37 °C for 1 h. For combined treatments, RBCs were first treated with mβCD for 30 min at 37 °C then with surfactin in the continued presence of mβCD for another 30 min. These RBCs were pelleted at 133 *g* for 2 min and gently resuspended in DMEM for adhesion to poly-L-lysine-coated coverslips. Alternatively, RBCs labeled with BODIPY-lipids (lipids*) were imaged during exposition to surfactins. To measure residual cholesterol, lipids were extracted and cholesterol was determined by Amplex Red Cholesterol kit (Invitrogen) in the absence of cholesterol esterase [22].

2.3. RBC labeling and vital imaging

RBCs were labeled with BODIPY-lipids (lipids*; Invitrogen) after spreading onto poly-L-lysine-coverslips. Briefly, cells were rinsed in DMEM and labeled at 20 °C for 15 min with 0.75 μM SM* or 1 μM PC* or 1 μM GlcCer* (except otherwise stated) in DMEM containing equimolar defatted bovine serum albumin (DF-BSA; Sigma) [26]. For confocal imaging, coverslips were placed bottom-up into Lab-Tek chambers and examined in the green channel with a Zeiss LSM510 confocal microscope using a plan-Apochromat 63x NA 1.4 oil immersion objective in a thermostated cabinet set at 37 ± 1 °C (XL/LSM incubator, Zeiss; Tempcontrol 37-2, PeCon) [26]. For excimer studies, RBCs were excited at 488 nm and images were simultaneously acquired in the green (λ_{em} 520 nm) and red channels (λ_{em} 605 nm) [27].

2.4. Hemolysis

Hemolysis was evaluated at 0.5 μM surfactins by hemoglobin release [22,38]. 0.2% Triton X-100 induced complete hemolysis, yielding the 100% control value.

2.5. Thin layer chromatography

Lipids* were inserted in the RBC membrane at 0.75 or 1 μM. After washing, all lipids (endogenous and inserted*) were extracted, separated by thin layer chromatography (TLC) in chloroform:methanol:15 mM $CaCl_2$ (65:35:8; v/v/v) [39] and revealed by charring densitometry after staining with 10% cupric sulfate in 8% O-phosphoric acid [40]. Band intensity of inserted lipid* was quantified and expressed by reference to the sum of major lipids (cholesterol, PC, phosphatidylethanolamine, ceramide and SM) from the same sample, after correction for band intensity of corresponding endogenous lipid.

2.6. Statistical analyses

Values are means ± SEM. Statistical significance of comparisons was tested by Student's *t* test. NS, not significant; *, $p < 0.05$; **, $p < 0.01$; and ***, $p < 0.001$.

3. Results

3.1. Micrometric lipid* domains in control RBCs are restricted by RBC stretching and membrane:cytoskeleton anchorage but favored by cholesterol

Using vital confocal imaging, we recently reported that fluorescent lipid analogs of glycosphingolipids (e.g. BODIPY-GlcCer [GlcCer*]), sphingomyelin (BODIPY-SM [SM*]) and phosphatidylcholine (BODIPY-PC [PC*]) spontaneously form (sub)micrometric domains at the plasma membrane (PM) of living RBCs adherent onto poly-L-lysine (PLK)-coated coverslips and of CHO cells (for lipid analog structures, see [26,27]). These domains are (i) readily visible on RBCs partially spread onto PLK-coated-coverslips, (ii) structurally and kinetically distinct, (iii) of decreasing packing: GlcCer* > SM* > PC*, and (iv) preferentially found at the outer PM leaflet, as revealed by their complete disappearance upon surface back-exchange by BSA (data not shown). Domains are probe concentration-independent, since increasing SM* concentration from 0.5 to 3 μM changed neither the number nor the size of domains (data not shown; [22]). The relation with endogenous lipid compartmentation has been discussed elsewhere [22,26,27].

All micrometric lipid* domains are strongly dependent on membrane tension since they can be seen on RBCs partially spread on the coverslip but not in most spread cells (see Fig. 1A, a). Moreover, domains are numerous when RBCs are barely attached, decline to a stable low number at partial spreading, and vanish upon maximal stretching [22]. Interestingly, they (re-)appear or increase in size upon incubation into mildly hypotonic medium (data not shown; [26]). In addition, domains are differentially restricted by membrane:cytoskeleton anchorage [22], presumably preventing domain increase in size and number. Accordingly, we observed that the combination of membrane:cytoskeleton uncoupling at 4.1R complexes upon PKC activation and membrane relaxation by incubation in mildly hypotonic medium led to a strong increase of GlcCer* domain abundance in comparison to control RBCs (data not shown). In contrast to membrane:cytoskeleton anchorage which restricts domains, cholesterol appears as a stabilization factor for PC* and SM* domains [22].

3.2. Cyclic natural surfactin-C_{13}–C_{15} promotes PC* and SM*, but not GSLs*, micrometric domains

Because membrane:surfactin interaction was so far mainly studied on model membranes containing mixtures of phosphatidylcholines with various acyl chain lengths and saturation levels [3,41,42], we first examined if surfactin, a natural mixture of 13, 14 and 15C-acyl chain lengths (surfactin-C_{13}–C_{15}), could affect the less-packed PC* micrometric domains when applied at concentrations <1 μM, i.e. well below the critical micellar concentration ([3,43]; see Suppl. Table 1). As previously reported [22], PC* analogs labeled (sub)micrometric domains on control RBCs partially spread on the coverslip (typically <8 μm in diameter; arrowheads at Fig. 1A, a), but not in most spread cells (arrows at Fig. 1A, a), presumably due to high membrane tension. When RBCs were preincubated for 30 min with 0.5 μM surfactin, PC* domain abundance was increased by ~2-fold (Fig. 1A, b; quantification at Fig. 2B). The effect of surfactin can be attributed neither to drug toxicity (no hemolysis was observed; data not shown) nor to an increased insertion of PC* in the RBC membrane, as evaluated by thin layer chromatography (data not shown). The kinetics of domain induction was monitored by time-lapse imaging on stage in cells prelabeled with PC*. To minimize photobleaching, a slightly higher surfactin concentration was used (0.75 μM instead of 0.5 μM). Induction of new PC* micrometric domains by surfactin was obvious but slow (Fig. 1B). Thus, like incubation in mildly hypotonic medium or membrane:cytoskeleton uncoupling (see Section 3.1), surfactin increases the abundance of PC* domains.

To further address if the effect of low (up to 1 μM) concentrations of surfactin on micrometric domains depended on lipid* domain packing, we next looked at the more packed SM* and GlcCer* domains [27]. As shown in Fig. 2, surfactin also increased the abundance of SM* domains (Fig. 2A, i, j), but not that of GlcCer* domains (Fig. 2A, k–o). The effect was concentration-dependent, peaking at 0.5 μM for PC* (Fig. 2A, c) vs 0.75 μM for SM* (Fig. 2A, i). Thus, surfactin best promoted domains for the less packed lipid analogs (PC* > SM*), without detectable effect on most packed GSLs*.

3.3. Surfactin-C_{13}–C_{15} reverses the attrition of PC* and SM* domains induced by cholesterol depletion

Because of the high cholesterol concentration of RBCs and the highest vulnerability of less packed domains to marginal cholesterol

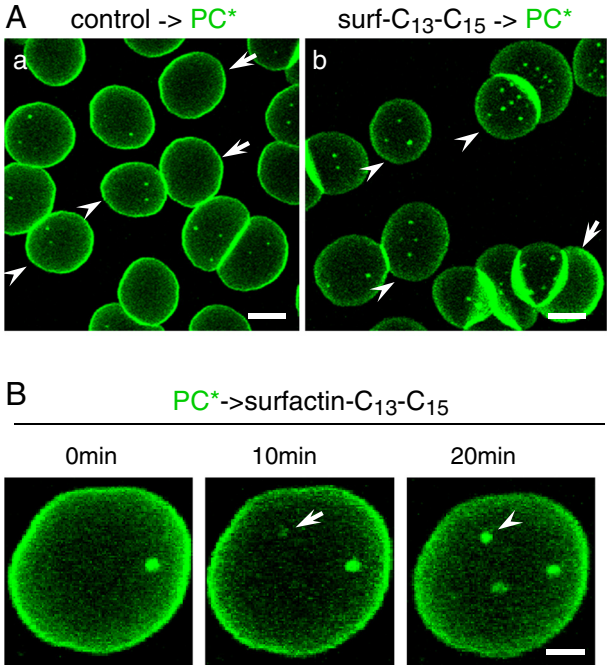

Fig. 1. In adherent RBCs, natural cyclic surfactin-C_{13}–C_{15} increases the abundance of BODIPY-PC (PC*) micrometric domains. (A) Vital imaging of RBCs preincubated with surfactin. Freshly isolated RBCs were either preincubated in suspension with 0.5 μM surfactin for 30 min (b) or kept untreated (a), then attached onto poly-L-lysine (PLK)-coated coverslips for 4 min and allowed to spread for additional 4 min, labeled with PC*, washed and immediately imaged at 37 °C. Notice at left that PC* labels several micrometric domains on partially spread cells (<8 μm; arrowheads) but not on more spread cells (arrows). At right, the number of domains is increased by surfactin, including on highly spread cells. Scale bars, 5 μm. (B) Time-lapse vital imaging of RBCs incubated on stage with surfactin. RBCs were attached–spread on PLK-coverslips as above, labeled with PC*, washed and imaged at 37 °C following the addition of 0.75 μM surfactin. Notice progressive domain appearance (arrow) and enlargement (arrowhead). Scale bar, 2 μm.

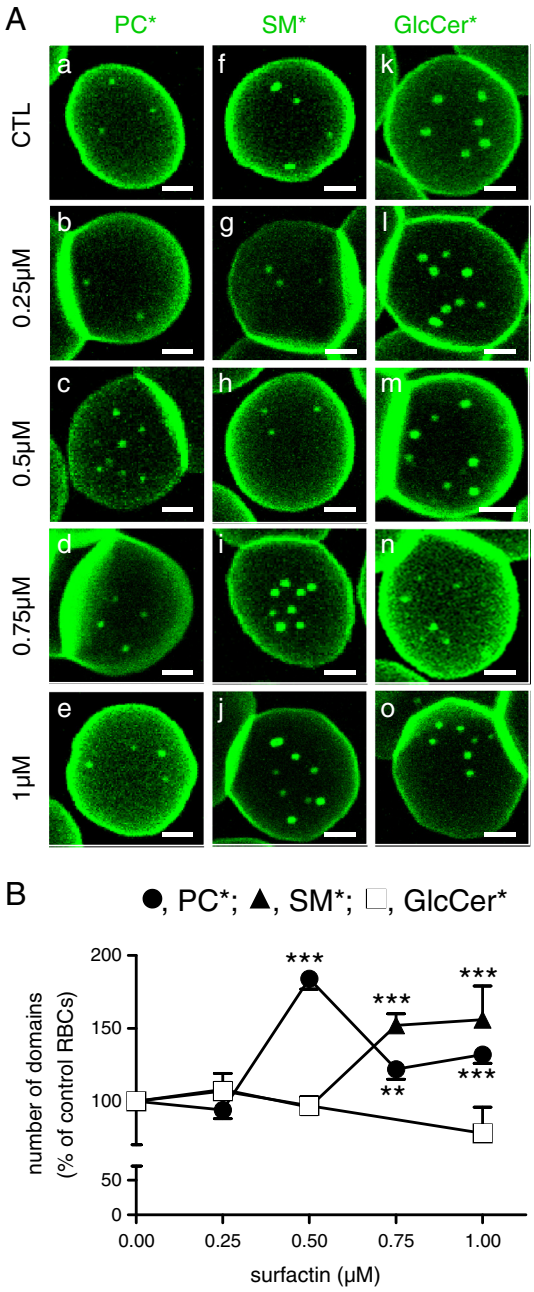

Fig. 2. Surfactin-C_{13}–C_{15} favors PC* and SM*, but not GlcCer*, domains in a concentration-dependent manner. (A) Representative confocal images. Freshly isolated RBCs were preincubated (b–e; g–j; l–o) or not (a, f, k) in suspension with the indicated concentration of surfactin-C_{13}–C_{15} for 30 min, attached–spread onto PLK-coverslips, labeled with PC* (a–e), SM* (f–j), or GlcCer* (k–o), washed and immediately imaged at 37 °C, as in Fig. 1. Notice the selective increase of PC* (c–e) and SM* domains upon surfactin (i, j), with different peak concentrations (0.5 μM surfactin for PC* and 0.75 μM for SM*); the abundance of GlcCer* domains is unchanged. All scale bars, 2 μm. (B) Morphometry. Micrometric domains are means ± SEM of (i) 44–664 RBCs for PC*; (ii) 23–322 RBCs for SM*; and (iii) 99–316 for GlcCer*, pooled from 4 independent experiments and normalized to untreated RBCs taken as 100%.

depletion [22], we thus asked whether surfactin can overcome the effect of cholesterol depletion. To this aim, we induced a moderate cholesterol depletion (~25%) by 0.25 mM methyl-β-cyclodextrin (mβCD), which causes complete attrition of PC* and SM*, but largely preserves GlcCer*, domains ([22]; Fig. 3A, c, g and quantification at Fig. 3B). Exposure of mβCD-treated RBCs to surfactin not only prevented disappearance of PC* and SM* domains but further increased the abundance of PC* domains by >3-fold as compared to untreated control RBCs (Fig. 3A; quantification at Fig. 3B; film at Fig. 3C). These results indicated that surfactin can substitute cholesterol to favor PC* and SM* micrometric domains or that both act in concert.

3.4. Surfactin-C_{13}–C_{15} increases excimer formation at PC* and SM* domains

Based on the reversion by surfactin of the attrition of PC* and SM* domains induced by mβCD, we then ask more directly whether the lipopeptide could, like cholesterol, affect lipid* domain organization. To this aim, we looked at clustering-dependent shift of BODIPY spectral properties, known as excimer formation [27]. This phenomenon results from a partial conversion of the primary emission peak at λ_{em} 520 nm (green) to a secondary emission at 605 nm (red). We therefore looked at green and red fluorescence emission from PC* and SM* domains, either at usual concentrations (Fig. 4a–d) or at higher SM* concentration to sensitize excimer formation ([23,26,27]; Fig. 4e). In control RBCs, no significant excimer formation was detected by line scans at the usual PC* and SM* concentration (Fig. 4a, c), but the phenomenon was obvious upon image inspection at 3 μM SM* (Fig. 4e, right, arrowheads) and can be quantified by line scan (up to ~25% red/green emission ratio; Fig. 4e′). Upon treatment with surfactin-C_{13}–C_{15}, excimer formation of cells exposed to 1 μM PC* or 0.75 μM SM* became detectable (arrowheads at panels b,d, right; compare with panels a, c), reaching emission ratios of ~15% (Fig. 4b′, d′).

3.5. Synthetic surfactins increase PC* domain abundance in an acyl chain length-dependent manner

Having shown that the mixture known as surfactin-C_{13}–C_{15} affected PC* and SM* domains in a cholesterol-sensitive manner, we next aimed at identifying the structural features of the surfactin molecule responsible for this effect. To this aim, several surfactins were compared: (i) purified natural cyclic surfactin with uniform acyl chain length of 14C (referred as SNC14); (ii) linear analogs with the same 14C-acyl chain and further differing in charge (2 vs 3 acid groups), referred as SAL14 and SSL14; and (iii) linear analogs differing in acyl chain length (10 vs 14 vs 18 carbons), referred as SSL10, SSL14 and SSL18 (for structures and characteristics, see Suppl. Fig. 1 and Suppl. Table 1, respectively). All congeners were used at the same concentrations as natural cyclic surfactin-C_{13}–C_{15} and none caused any hemolysis (data not shown).

Irrespective of their geometry (cyclic vs linear) and charge (2 vs 3), all tested surfactins with 14C (purified natural cyclic SNC14 as well as the linear SAL14 and SSL14 with respectively 2 and 3 negative charges) increased by ~2-fold the number of PC* domains (Fig. 5A, b, c, h), like natural surfactin mixture with 13 to 15C. This indicated that surfactin overall geometry and charge density were not determinant factors for drug effect on PC* micrometric domains. In contrast, increasing surfactin acyl chain length from 10 (SSL10) to 14 (SSL14) to 18C (SSL18) differentially increased PC* domain abundance, from ~1.5-fold to ~3-fold as compared to control cells (panels g, h, i at Fig. 5A and quantification at Fig. 5B, upper panel), indicating that surfactin acyl chain length is instead a key determinant for the increase of PC* micrometric domains.

3.6. Relation between synthetic surfactin acyl chain length and the increase of PC* domain abundance is inverted upon cholesterol depletion

Next, to evaluate if all tested surfactins can overcome the attrition of PC* domains induced by cholesterol depletion, a similar experiment was performed after the removal of ~25% cholesterol by 0.25 mM mβCD [22]. Like natural cyclic surfactin-C_{13}–C_{15}, purified cyclic surfactin SNC14 and synthetic linear compounds (SAL14, SSL10-18), whatever their geometry, charge and acyl chain length, suppressed the effect of cholesterol depletion on PC* domains (Fig. 5A, +mβCD). However, while surfactin with the longest acyl chain (SSL18) induced the strongest increase of PC* domain abundance in RBCs with normal cholesterol content (see Fig. 5, −mβCD), the opposite was observed in RBCs treated with mβCD (Fig. 5B, lower panel). Altogether, these results

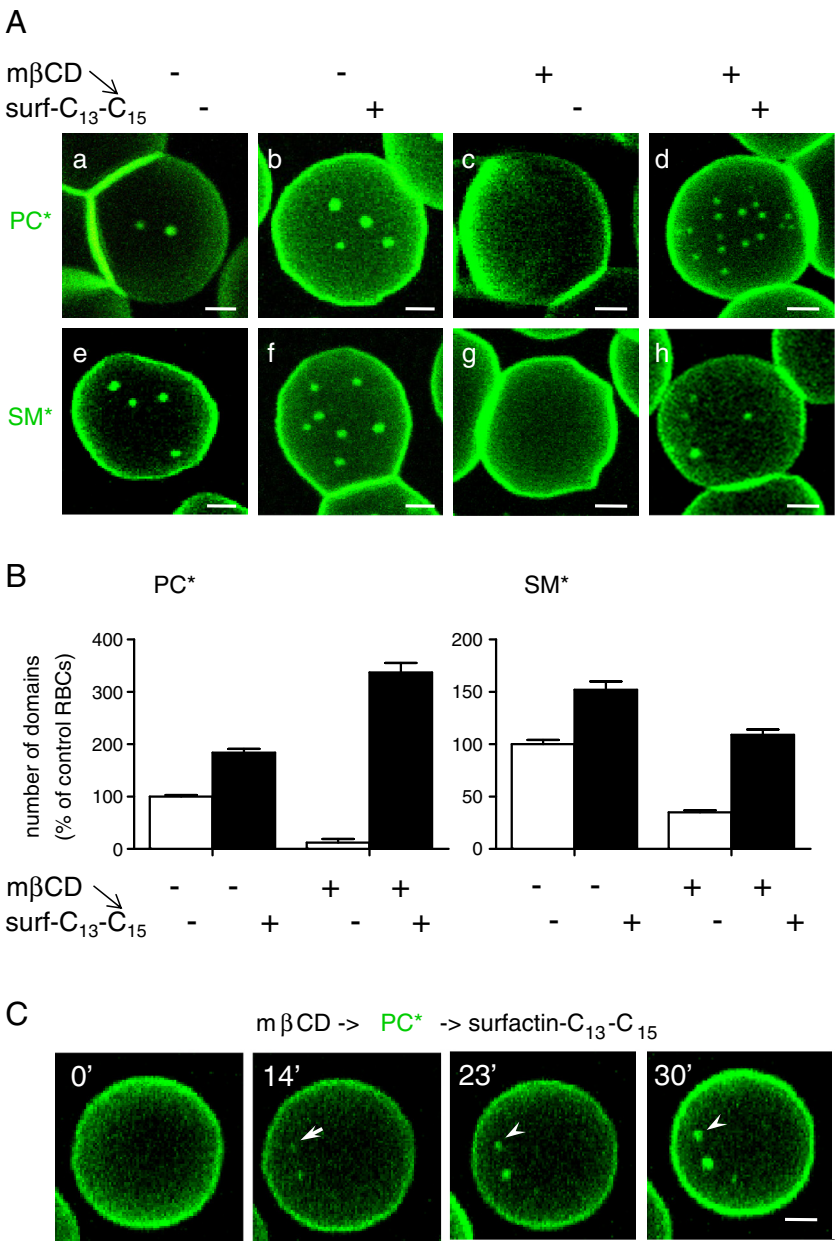

Fig. 3. Surfactin-C_{13}–C_{15} reverses the attrition of PC* and SM* domains induced by cholesterol depletion. (A) Representative confocal images. Freshly isolated RBCs were preincubated (c, d, g, h) or not (a, b, e, f) in suspension with 0.25 mM methyl-β-cyclodextrin (mβCD) for 1 h to decrease endogenous cholesterol by ~25%. During the last 30 min, RBCs were further exposed to 0.5 μM (b, d) or 0.75 μM (f, h) surfactin, in the continued presence of mβCD if appropriate. RBCs were then attached–spread onto PLK-coverslips, labeled as above with PC* (a–d) or SM* (e–h), washed and immediately imaged at 37 °C. Note that the disappearance of PC* and SM* domains by moderate cholesterol depletion (c, g) is reversed by surfactin. For PC* domains, number is even increased by ~3-fold in comparison to control cells. All scale bars, 2 μm. (B) Morphometry. PC* (left panel) and SM* (right panel) domains upon combined treatment with mβCD and surfactin are means ± SEM of 288 and 258 RBCs pooled from 3 independent experiments, as percentage of untreated control cells. (C) Time-lapse vital imaging of mβCD-treated RBC incubated on stage with surfactin. Freshly isolated RBCs were preincubated for 30 min with 0.25 mM mβCD, then attached–spread onto PLK-coverslips, labeled with PC*, washed and imaged by confocal microscopy at 37 °C upon treatment with 0.75 μM surfactin for the indicated times. Notice progressive domain appearance (arrow) and enlargement (arrowheads). Scale bar, 2 μm.

indicate that surfactin analogs increased PC* domain abundance in an acyl chain length-dependent manner and that cholesterol depletion inverted this tendency, suggesting that membrane:surfactin analog interaction depends on endogenous cholesterol level.

3.7. Synthetic surfactins also affect SM domain abundance in an acyl chain length-dependent manner*

Because synthetic surfactins can substitute cholesterol to support PC* micrometric domains, we then asked whether and how synthetic surfactins could also affect the more packed SM* domains [27]. Whereas no effect was observed in RBCs incubated with SNC14 and SAL14 (Fig. 6A, b, c), acyl chain length differentially influenced SM* domain abundance, from a ~1.5-fold decrease for the short SSL10 to a ~1.5-fold increase for the long SSL18 (Fig. 6A, d–f; quantification at Fig. 6B). Moreover, removing cholesterol inverted this tendency, as observed on PC* domains: the longest acyl chain length, the lowest SM* domain abundance (data not shown). Thus, like for PC* domains, SM* domain abundance can be modulated by surfactin acyl chain length. However, in contrast to PC* domains, the effect on SM* domain abundance was differential: decreased by short surfactins (SSL10) but promoted by long surfactins (SSL18).

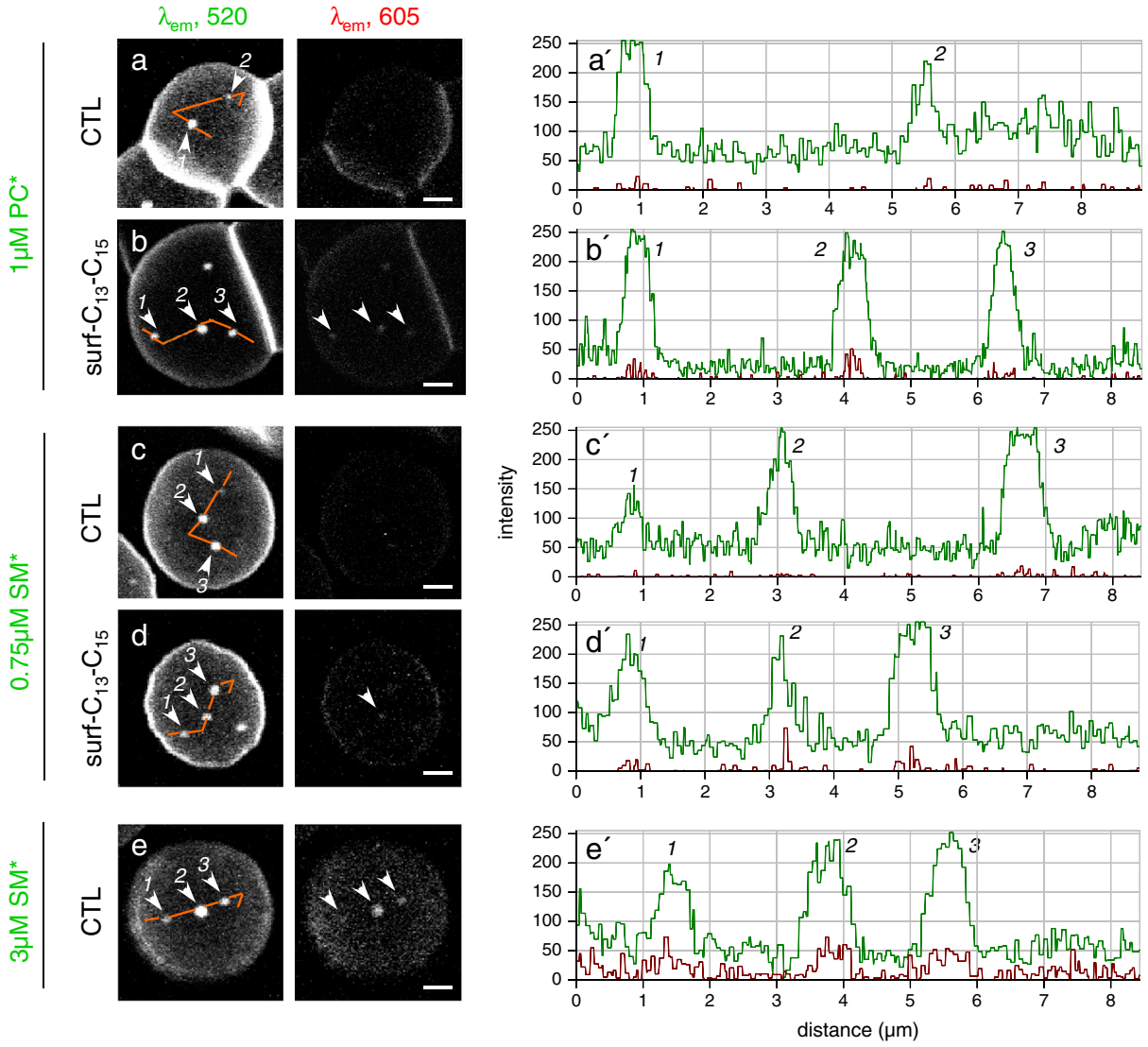

Fig. 4. Surfactin-C_{13}–C_{15} induces a spectral shift ("excimers") of PC* and SM* domains. Left, confocal imaging. Freshly isolated RBCs were incubated (b, d) or not (a, c, e) in suspension with surfactin-C_{13}–C_{15} at 0.5 μM (b) or 0.75 μM (d) for 30 min, then attached onto PLK-coverslips, labeled with PC* at 1 μM (usual concentration; a, b) or with SM* at either 0.75 μM (usual concentration; c, d) or 3 μM to sensitize excimer formation (e), washed and immediately examined by confocal microscopy. All images were generated with λ_{exc} 488 nm, with simultaneous recording in the green (left; λ_{em} 520 nm) and red channels (right; λ_{em} 605 nm). Signal in red images (right) is indicative of packed clustering (excimers). Notice that excimers are totally absent in control RBCs incubated with 1 μM PC* (a) and 0.75 μM SM* (c) but induced by surfactin-C_{13}–C_{15} (b, d) and best seen with 3 μM SM* in control RBCs (e). All scale bars, 2 μm. Right, quantitation of conventional (green) and excimer emission (red). Intensity profiles were recorded along the paths indicated by continuous orange lines at left. Numbers 1–3 refer to the indicated patches. Average red/green emission ratio for PC* and SM* in control RBCs is <5% at usual lipid* concentrations (a′, c′), reaches ~15% upon incubation with surfactin-C_{13}–C_{15} (b, d), and up to ~25% at 3 μM SM* without surfactin (e′).

4. Discussion

4.1. Current model for micrometric BODIPY-lipid domain biogenesis and (co-)existence in control RBCs

Before discussing how surfactin affects lipid* domain organization and abundance, let us summarize our current view, based on this paper and our previous studies [22,26,27], for micrometric lipid* domain (i) biogenesis; (ii) low cell surface coverage and round shape; (iii) coexistence; and (iv) relevance for endogenous lipids.

Whereas micrometric lipid domains are observed with all the three classes of polar lipids* used, i.e. GSLs*, SM* and PC*, their abundance is differentially controlled by stabilization and restriction machineries. Thus, GlcCer* domains are favored by high temperature and ankyrin complexes, whereas PC* and SM* domains are promoted by cholesterol and regulated linkage to the 4.1R complex [22,26,27]. Moreover, our studies point to three differences between PC* and SM* domains: (i) their intrinsic propensity to form excimers (SM* but not PC*); (ii) their interaction with 4.1R complexes, providing either internal stabilization (SM*) or peripheral retention (PC*); and (iii) their control by cholesterol, as regulator of membrane fluidity (SM*) or membrane:cytoskeleton anchorage (SM* and PC*) [22,26,27]. In contrast, membrane stretching and membrane:cytoskeleton anchorage constitute restriction factors for domains, thereby preventing domain expansion [22,27]. Biophysical studies should address the mechanical parameters governing the relation between membrane tension and lipid* domain packing and size in RBCs. Nevertheless, phase coexistence at the rabbit RBC membrane studied by multiphoton microscopy after labeling with LAURDAN allows evidencing tightly packed domains, with different lipid packing and sizes, moving in a more fluid background phase [35].

High membrane stretching and strong membrane:cytoskeleton anchorage in RBCs, which constitute restriction factors for lipid* micrometric domains thereby preventing domain expansion [22],

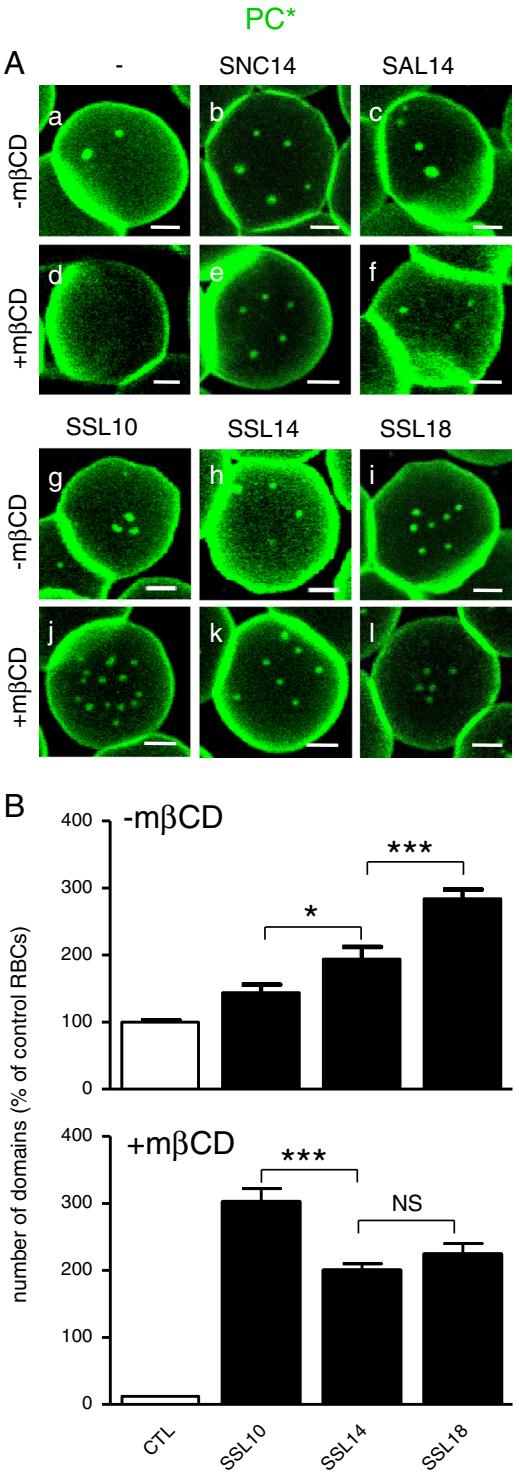

Fig. 5. Synthetic linear surfactins modulate PC* domain abundance in an acyl chain length- and cholesterol-dependent manner. (A) Confocal imaging for several cyclic and linear surfactins. Freshly isolated RBCs were preincubated in suspension with 0.25 mM mβCD for 1 h (d–f; j–l) or not (a–c; g–i). During the last 30 min, cells were further exposed to the indicated surfactins (SNC14, *S*urfactin *N*atural *C*yclic with *14*C-acyl chain length; SAL14, *S*urfactin *A*cylated *L*inear with *14*C; SSL10, SSL14 and SSL18, *S*urfactin *S*ynthetic *L*inear with *10*, *14* and *18*C, respectively) at 0.5 μM for 30 min in the continued presence of mβCD if appropriate. RBCs were attached-spread onto PLK-coverslips, labeled with PC*, washed and immediately imaged by confocal microscopy at 37 °C. All scale bars, 2 μm. (B) Morphometry for synthetic linear surfactins with various acyl chain lengths. Data are means ± SEM of 53–421 RBCs pooled from 2–3 experiments and are expressed as percentage of untreated control cells.

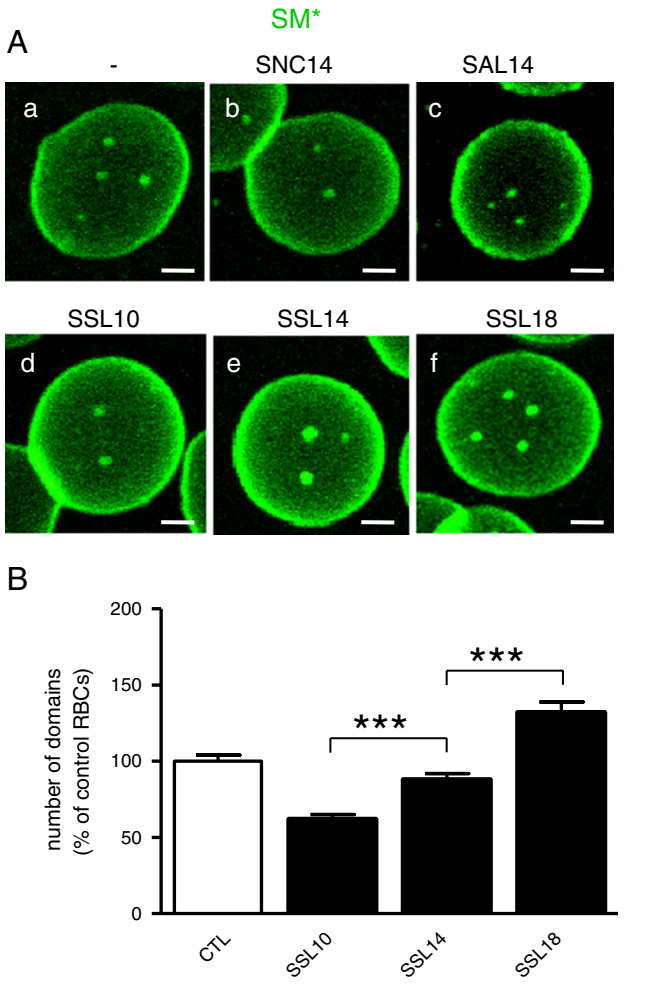

Fig. 6. Synthetic linear surfactins modulate SM* domain abundance in an acyl chain length-dependent manner. (A) Confocal imaging for several cyclic and linear surfactins. Freshly isolated RBCs were incubated or not (a) in suspension with the same surfactins as in Fig. 5, at 0.75 μM for 30 min, then attached–spread onto PLK-coverslips, labeled with SM*, washed and immediately imaged at 37 °C. All scale bars, 2 μm. (B) Morphometry for synthetic linear surfactins with various acyl chain lengths. SM* domains are means ± SEM of 135–361 RBCs pooled from 2–4 independent experiments and are expressed as percentage of untreated control cells.

could explain the lower coverage by domains of the RBC vs CHO cell surface, ~7% vs ~25% respectively [26,27]. Furthermore, high membrane tension in RBCs could also restrict lipid domains into round shape, in order to decrease domain line tension, and could explain why lipid* domains are more round in RBCs than in fibroblasts [26,27].

Based on double-labeling experiments, differential membrane: cytoskeleton anchorage and differential effect of temperature, we have previously suggested that the RBC PM is organized in at least three segregated lipid* domains. However, only a fraction of the lipids* at the PM is present in the round micrometric lipid* domains and three lines of evidence support the existence of a surrounding phase. First, considering that SM* domains cover ~7% of the PM, their ~8-fold enrichment indicates that about half of the SM* is present in the domains and the other half outside [26]. Second, the three classes of lipids* show a distinct number of domains according to the temperature: whereas GlcCer* shows an increasing domain number when temperature is increased from 20 °C to 37 °C, SM* and PC* show a peak of domains at 20 °C and a strong decrease thereafter; accordingly, a weak and homogenous labeling with PC* can also be detected at 37 °C [27]. Third, although domains are immobile, they show a very fast recovery after photobleaching, indicating that domains* are large-scale immobile assemblies of highly dynamic individual or small clusters of lipids*.

Relevance of fluorescent lipid* domains for endogenous lipids is supported by three observations: (i) co-localization of exogenous GM1* with endogenous GM1 labeled with subunit B cholera toxin in RBCs; (ii) identity of PM domains in CHO cells upon insertion of SM* vs metabolic conversion of ceramide* into SM* at physiological temperature; and (iii) selective disappearance of SM* upon endogenous SM depletion [22,26,27].

4.2. Preferential formation by surfactin of less-packed PC* and SM* domains

As shown by live cell imaging of RBCs, low concentrations of surfactin induced the formation of new PC* and SM* micrometric domains, without obvious effect on GlcCer* domains. Based on the complete abolishment of RBC PC* and SM* labeling upon back-exchange with BSA (data not shown) and on the very limited flip-flop of surfactin from outer to inner leaflet [42], the increased abundance of domains induced by surfactin should be due to PC* and SM* clustering from the surrounding lipid* pool in the outer PM leaflet. By FRAP experiments in RBCs, we indeed observed very fast ($t_{1/2}$ ~ 10 s) and high recovery of PC* and SM* domain constituents [22]. Assuming a representative behavior of the surfaces we analyzed, area estimations indicate that SM* domains account from ~7% of the RBC surface at 20 °C. The respective ~8-fold enrichment in these micrometric domains indicates that about half of total SM* would be clustered in these domains and half outside [26].

Although PC* and SM* differ from GlcCer* by the same small and zwitterionic phosphocholine headgroup, this explanation for a differential effect of surfactin is not satisfactory because: (i) whereas surfactin reversed the attrition of SM* domains induced by moderate cholesterol depletion, it increased by >3-fold PC* domain abundance in comparison to control RBCs; and (ii) changing the charge number of synthetic surfactins (SAL14 with 2 charges vs SSL14 with 3 charges) had no effect on the increase of PC* domain abundance.

Besides differences in polar headgroup size and charge, PC* and SM* domains show a lower propensity than GlcCer* to form excimers [23,26,27]. Because surfactin preferentially increased the abundance of PC* and SM* domains, we favor the view that the drug preferentially interacts with less-packed lipid* domains. This proposal in living cells fits with the observation that surfactin shows a stronger insertion in mixed monolayers containing phospholipids with short chain length and/or in a fluid-like organization [42]. In another study, binding affinity of surfactin to LUVs was higher for S_o- than L_d- than L_o-phases [44], again in agreement with our data on RBCs in which L_d/S_o phases are not expected to coexist due to their very high cholesterol content [45].

A third difference between lipid* micrometric domains is unequal sensitivity to cholesterol depletion, higher for PC* and SM* than for GlcCer* domains. We will now discuss how surfactin could interact with membranes, by systematic comparison with the well-known effects of cholesterol on biological membranes.

4.3. Cholesterol-like effects of surfactin

Two lines of evidence indicate that surfactin and cholesterol similarly impact on micrometric domains: (i) cholesterol depletion by mβCD and surfactin addition oppositely affected both PC* and SM* domain abundance; and (ii) disappearance of PC* and SM* domains by mβCD was completely abrogated by surfactin. The hypothesis of cholesterol-like effect of surfactin will guide a further discussion on how surfactin could affect membrane lateral organization in micrometric domains. Cholesterol not only regulates membrane fluidity at a global level but also favors biogenesis of micrometric lipid domains at discrete predefined spots by promoting intrinsic polar lipid packing [22,27]. Cholesterol apparently concentrates at the boundaries between liquid and gel-like phases, thereby reducing line tension [46]. Cholesterol was also reported to modulate membrane:cytoskeleton coupling [22,36,47], but this is poorly relevant for surfactins for which flip-flop from the outer to the inner leaflet is very limited [42,48]. Arguing against a modulation by surfactin of global membrane fluidity, the three classes of polar lipids* were differentially affected by surfactin, in agreement with the recent classification of surfactin into the group of heterogeneously-perturbing surfactants which disrupt membrane locally [49]. We thus favor the view that surfactin promotes biogenesis specifically at PC* and SM* domains. We indeed observed a specific increased abundance and excimer formation from these two domains. Increased excimer formation might reflect that (i) lipid* domains got fewer or smaller; (ii) lipids* showed a stronger preference for domains; and/or (iii) lipid* diffusion and molecular motions within the domains were enhanced. Based on increased domain abundance and size, the first hypothesis can be ruled out. The effect of surfactin on domain abundance and excimer formation would thus probably be due to a combination of the two latter hypotheses and could be explained by a strengthening of hydrophobic interactions between acyl chains of lipids and surfactins, reminiscent to the wedge-like shapes of SLs and cholesterol that allow them to come in very close apposition via van der Waals forces [50]. Similarly, sphingosine, which also behaves as a surface-active amphiphile, rigidifies pre-existing gel domains in mixed bilayers [15,51,52]. We also noticed that small changes of surfactin concentrations lead to contrasting effects on lipid* domains, with a peak at 0.5 μM and a subsequent decrease for PC* domains, with concomitant increase of SM* domains. This concentration effect could be explained by a shift of surfactin interaction, first with PC* domains, then with SM* domains and/or at domain boundaries, thereby reducing line tension at interface and eroding domains.

If this view is correct, then high local cholesterol concentrations would prevent any effect of surfactin. This prediction is consistent with the higher increase of PC* domains abundance by surfactin in RBCs with lower cholesterol level vs normal RBCs. Accordingly, it has been shown that the presence of cholesterol in the phospholipid membrane attenuates the destabilizing effect of surfactins [53] and that surfactin preferentially lyses cholesterol-free liposomes [54]. However, it seems at first glance inconsistent with the absence of effect of addition of stigmasterol on surfactin interaction with LUVs [44]. This apparent discrepancy might be explained by the very low level of stigmasterol used in the latter study and/or by the ability of cholesterol, but not stigmasterol, to form domains in DOPC/SM bilayers [55]. The higher impact of surfactin on RBCs when cholesterol content was decreased markedly contrasts to the behavior of other lipopeptides produced by *Bacillus* species, such as fengycin, iturins and mycosubtilin, which show high affinity for cholesterol [56–58] via a tyrosyl residue [56]. Thus, whereas surfactin could substitute cholesterol, the latter three drugs depend on it.

4.4. Critical surfactin structural features involved in micrometric lipid* domain modulation

To prevent hemolysis, Dufour and collaborators have synthesized various linear surfactin analogs differing by charge and hydrophobicity (for structures and characteristics, see Suppl. Fig. 1 and Suppl. Table 1, respectively). Whereas surfactin geometry and charge density did not impact on fluorescent lipid lateral compartmentation in domains, the acyl chain length was an important feature: the longest the chain (SSL18), the highest the increase of PC* and SM* domain abundance. This observation perfectly agrees with the highest insertion into DPPC monolayer of surfactins bearing the longest acyl chain (Suppl. Table 1). However, an opposite effect was observed in RBCs partially depleted in cholesterol: the shortest the acyl chain, the highest the increase of PC* and SM* domain abundance. This raises the possibility that cholesterol removal could leave room for the small SSL10. These observations underline that, besides surfactin structural features, host membrane composition, e.g. cholesterol abundance, is a key parameter for membrane:surfactin interaction, and must be kept in mind for designing new surfactins.

4.5. Model for surfactin:membrane interaction and surface activity, based on surfactin structural features and host membrane composition/organization

An inverse relation can be established between critical micellar concentration of linear surfactin analogs (CMC, 1114 vs 302 vs 8 for SSL10, SSL14 and SSL18 respectively; see Suppl. Table 1) [41] and micrometric lipid* domain abundance in normal RBCs: the lowest the CMC, the highest the domain abundance; moreover, this relation was inverted upon cholesterol depletion. We thus propose a new model for surfactin:membrane interaction based on lipid domain organization and cholesterol abundance/distribution. In RBCs with normal cholesterol level, long surfactins (e.g. SSL18) would preferentially insert inside domains, because of deep insertion into the hydrophobic core of the membrane, while short surfactins (e.g. SSL10) could only find their place at domain boundary, as already proposed [42], reducing line tension and domain size. Accordingly, SSL10 did not increase but decreased SM* domain abundance, in contrast to natural cyclic surfactin. However, when cholesterol was removed, the short chain SSL10 showed a stronger increase of PC* domains, which would further gain access inside domains and substitute cholesterol, thereby favoring domain coalescence.

4.6. Conclusion

Taken together, our data imply that, in addition to surfactin structure and concentration, the modulation of the lateral organization of PM fluorescent lipids by surfactin appears dictated by lipid* domain packing and sterol content. The preference for membranes with a lower global cholesterol content and for domains with low packing could explain why surfactin preferentially disrupts bacterial membranes since prokaryotic membranes almost universally lack sterols and SLs [59]. This contrasts with the poor toxicity of surfactin to fungi and plant membranes [44] that contain high sterol, inositolphosphorylglycolipids and glycosphingolipids and show lateral compartmentation in micrometric domains [59,60]. In conclusion, the cholesterol content of the host membrane and its organization in domains must be taken into account to evaluate surfactin surface activity and toxicity and for designing new surfactin analogs.

Supplementary data to this article can be found online at http://dx.doi.org/10.1016/j.bbamem.2013.05.006.

Acknowledgments

This work was supported by grants from the UCL (FSR), the F.R.S.-FNRS, the Région Wallonne, the Région Bruxelloise, the Salus Sanguinis Foundation, the Loterie Nationale, the ARC and the IUAP (Belgium). MD thanks the FNRS for her position as Research Associate.

References

[1] F. Peypoux, J.M. Bonmatin, J. Wallach, Recent trends in the biochemistry of surfactin, Appl. Microbiol. Biotechnol. 51 (1999) 553–563.
[2] R. Maget-Dana, M. Ptak, Interactions of surfactin with membrane models, Biophys. J. 68 (1995) 1937–1943.
[3] M. Deleu, J. Lorent, L. Lins, R. Brasseur, N. Braun, K. El Kirat, T. Nylander, Y.F. Dufrene, M.P. Mingeot-Leclercq, Effects of surfactin on membrane models displaying lipid phase separation, Biochim. Biophys. Acta 1828 (2012) 801–815.
[4] S. Dufour, M. Deleu, K. Nott, B. Wathelet, P. Thonart, M. Paquot, Hemolytic activity of new linear surfactin analogs in relation to their physico-chemical properties, Biochim. Biophys. Acta 1726 (2005) 87–95.
[5] G. van Meer, D.R. Voelker, G.W. Feigenson, Membrane lipids: where they are and how they behave, Nat. Rev. Mol. Cell Biol. 9 (2008) 112–124.
[6] S.J. Singer, G.L. Nicolson, The fluid mosaic model of the structure of cell membranes, Science 175 (1972) 720–731.
[7] D. Lingwood, K. Simons, Lipid rafts as a membrane-organizing principle, Science 327 (2010) 46–50.
[8] D. Lingwood, J. Ries, P. Schwille, K. Simons, Plasma membranes are poised for activation of raft phase coalescence at physiological temperature, Proc. Natl. Acad. Sci. U.S.A. 105 (2008) 10005–10010.
[9] L.J. Pike, Rafts defined: a report on the Keystone symposium on lipid rafts and cell function, J. Lipid Res. 47 (2006) 1597–1598.
[10] A. Fujita, J. Cheng, M. Hirakawa, K. Furukawa, S. Kusunoki, T. Fujimoto, Gangliosides GM1 and GM3 in the living cell membrane form clusters susceptible to cholesterol depletion and chilling, Mol. Biol. Cell 18 (2007) 2112–2122.
[11] H. Mizuno, M. Abe, P. Dedecker, A. Makino, S. Rocha, Y. Ohno-Iwashita, J. Hofkens, T. Kobayashi, A. Miyawaki, Fluorescent probes for superresolution imaging of lipid domains on the plasma membrane, Chem. Sci. 2 (2011) 1548–1553.
[12] L.A. Bagatolli, J.H. Ipsen, A.C. Simonsen, O.G. Mouritsen, An outlook on organization of lipids in membranes: searching for a realistic connection with the organization of biological membranes, Prog. Lipid Res. 49 (2010) 378–389.
[13] N. Kahya, D. Scherfeld, K. Bacia, B. Poolman, P. Schwille, Probing lipid mobility of raft-exhibiting model membranes by fluorescence correlation spectroscopy, J. Biol. Chem. 278 (2003) 28109–28115.
[14] T. Baumgart, S.T. Hess, W.W. Webb, Imaging coexisting fluid domains in biomembrane models coupling curvature and line tension, Nature 425 (2003) 821–824.
[15] F.M. Goni, A. Alonso, Effects of ceramide and other simple sphingolipids on membrane lateral structure, Biochim. Biophys. Acta 1788 (2009) 169–177.
[16] J.V. Busto, J. Sot, J. Requejo-Isidro, F.M. Goni, A. Alonso, Cholesterol displaces palmitoylceramide from its tight packing with palmitoylsphingomyelin in the absence of a liquid-disordered phase, Biophys. J. 99 (2010) 1119–1128.
[17] L.A. Bagatolli, To see or not to see: lateral organization of biological membranes and fluorescence microscopy, Biochim. Biophys. Acta 1758 (2006) 1541–1556.
[18] M. Edidin, The state of lipid rafts: from model membranes to cells, Annu. Rev. Biophys. Biomol. Struct. 32 (2003) 257–283.
[19] A. Kusumi, K.G. Suzuki, R.S. Kasai, K. Ritchie, T.K. Fujiwara, Hierarchical mesoscale domain organization of the plasma membrane, Trends Biochem. Sci. 36 (2011) 604–615.
[20] A. Kusumi, T.K. Fujiwara, R. Chadda, M. Xie, T.A. Tsunoyama, Z. Kalay, R.S. Kasai, K.G. Suzuki, Dynamic organizing principles of the plasma membrane that regulate signal transduction: commemorating the fortieth anniversary of singer and Nicolson's fluid-mosaic model, Annu. Rev. Cell Dev. Biol. 28 (2012) 215–250.
[21] T. Fujiwara, K. Ritchie, H. Murakoshi, K. Jacobson, A. Kusumi, Phospholipids undergo hop diffusion in compartmentalized cell membrane, J. Cell Biol. 157 (2002) 1071–1081.
[22] L. D'Auria, M. Fenaux, P. Aleksandrowicz, P. Van Der Smissen, C. Chantrain, C. Vermylen, M. Vikkula, P.J. Courtoy, D. Tyteca, Micrometric segregation of fluorescent membrane lipids: relevance for endogenous lipids and biogenesis in erythrocytes, J. Lipid Res. 54 (2013) 1066–1076.
[23] R.D. Singh, Y. Liu, C.L. Wheatley, E.L. Holicky, A. Makino, D.L. Marks, T. Kobayashi, G. Subramaniam, R. Bittman, R.E. Pagano, Caveolar endocytosis and microdomain association of a glycosphingolipid analog is dependent on its sphingosine stereochemistry, J. Biol. Chem. 281 (2006) 30660–30668.
[24] K. Gousset, W.F. Wolkers, N.M. Tsvetkova, A.E. Oliver, C.L. Field, N.J. Walker, J.H. Crowe, F. Tablin, Evidence for a physiological role for membrane rafts in human platelets, J. Cell. Physiol. 190 (2002) 117–128.
[25] M. Hao, S. Mukherjee, F.R. Maxfield, Cholesterol depletion induces large scale domain segregation in living cell membranes, Proc. Natl. Acad. Sci. U.S.A. 98 (2001) 13072–13077.
[26] D. Tyteca, L. D'Auria, P.V. Der Smissen, T. Medts, S. Carpentier, J.C. Monbaliu, P. de Diesbach, P.J. Courtoy, Three unrelated sphingomyelin analogs spontaneously cluster into plasma membrane micrometric domains, Biochim. Biophys. Acta 1798 (2010) 909–927.
[27] L. D'Auria, P. Van der Smissen, F. Bruyneel, P.J. Courtoy, D. Tyteca, Segregation of fluorescent membrane lipids into distinct micrometric domains: evidence for phase compartmentation of natural lipids? PLoS One 6 (2011) e17021.
[28] G. Grossmann, J. Malinsky, W. Stahlschmidt, M. Loibl, I. Weig-Meckl, W.B. Frommer, M. Opekarova, W. Tanner, Plasma membrane microdomains regulate turnover of transport proteins in yeast, J. Cell Biol. 183 (2008) 1075–1088.
[29] K. Malinska, J. Malinsky, M. Opekarova, W. Tanner, Visualization of protein compartmentation within the plasma membrane of living yeast cells, Mol. Biol. Cell 14 (2003) 4427–4436.
[30] J. Malinsky, M. Opekarova, W. Tanner, The lateral compartmentation of the yeast plasma membrane, Yeast 27 (2010) 473–478.
[31] F. Spira, N.S. Mueller, G. Beck, P. von Olshausen, J. Beig, R. Wedlich-Soldner, Patchwork organization of the yeast plasma membrane into numerous coexisting domains, Nat. Cell Biol. 14 (2012) 640–648.
[32] P.F. Devaux, R. Morris, Transmembrane asymmetry and lateral domains in biological membranes, Traffic 5 (2004) 241–246.
[33] A. Ciana, C. Achilli, C. Balduini, G. Minetti, On the association of lipid rafts to the spectrin skeleton in human erythrocytes, Biochim. Biophys. Acta 1808 (2011) 183–190.
[34] A. Ciana, C. Balduini, G. Minetti, Detergent-resistant membranes in human erythrocytes and their connection to the membrane–skeleton, J. Biosci. 30 (2005) 317–328.
[35] S.A. Sanchez, M.A. Tricerri, E. Gratton, Laurdan generalized polarization fluctuations measures membrane packing micro-heterogeneity in vivo, Proc. Natl. Acad. Sci. U.S.A. 109 (2012) 7314–7319.
[36] M. Sun, N. Northup, F. Marga, T. Huber, F.J. Byfield, I. Levitan, G. Forgacs, The effect of cellular cholesterol on membrane–cytoskeleton adhesion, J. Cell Sci. 120 (2007) 2223–2231.
[37] M. Salomao, X. Zhang, Y. Yang, S. Lee, J.H. Hartwig, J.A. Chasis, N. Mohandas, X. An, Protein 4.1R-dependent multiprotein complex: new insights into the structural organization of the red blood cell membrane, Proc. Natl. Acad. Sci. U.S.A. 105 (2008) 8026–8031.

[38] M.J. Parnham, H. Wetzig, Toxicity screening of liposomes, Chem. Phys. Lipids 64 (1993) 263–274.
[39] Z.J. Cheng, R.D. Singh, D.K. Sharma, E.L. Holicky, K. Hanada, D.L. Marks, R.E. Pagano, Distinct mechanisms of clathrin-independent endocytosis have unique sphingolipid requirements, Mol. Biol. Cell 17 (2006) 3197–3210.
[40] J.B. Marsh, D.B. Weinstein, Simple charring method for determination of lipids, J. Lipid Res. 7 (1966) 574–576.
[41] G. Francius, S. Dufour, M. Deleu, M. Paquot, M.P. Mingeot-Leclercq, Y.F. Dufrene, Nanoscale membrane activity of surfactins: influence of geometry, charge and hydrophobicity, Biochim. Biophys. Acta 1778 (2008) 2058–2068.
[42] O. Bouffioux, A. Berquand, M. Eeman, M. Paquot, Y.F. Dufrene, R. Brasseur, M. Deleu, Molecular organization of surfactin-phospholipid monolayers: effect of phospholipid chain length and polar head, Biochim. Biophys. Acta 1768 (2007) 1758–1768.
[43] H. Heerklotz, J. Seelig, Detergent-like action of the antibiotic peptide surfactin on lipid membranes, Biophys. J. 81 (2001) 1547–1554.
[44] G. Henry, M. Deleu, E. Jourdan, P. Thonart, M. Ongena, The bacterial lipopeptide surfactin targets the lipid fraction of the plant plasma membrane to trigger immune-related defence responses, Cell. Microbiol. 13 (2011) 1824–1837.
[45] W.F. Wolkers, L.M. Crowe, N.M. Tsvetkova, F. Tablin, J.H. Crowe, In situ assessment of erythrocyte membrane properties during cold storage, Mol. Membr. Biol. 19 (2002) 59–65.
[46] S. Mukherjee, F.R. Maxfield, Membrane domains, Annu. Rev. Cell Dev. Biol. 20 (2004) 839–866.
[47] F.J. Byfield, H. Aranda-Espinoza, V.G. Romanenko, G.H. Rothblat, I. Levitan, Cholesterol depletion increases membrane stiffness of aortic endothelial cells, Biophys. J. 87 (2004) 3336–3343.
[48] M. Deleu, O. Bouffioux, H. Razafindralambo, M. Paquot, C. Hbid, P. Thonart, P. Jacques, R. Brasseur, Interaction of surfactin with membranes: a computational approach, Langmuir 19 (2003) 3377–3385.
[49] M. Nazari, M. Kurdi, H. Heerklotz, Classifying surfactants with respect to their effect on lipid membrane order, Biophys. J. 102 (2012) 498–506.
[50] B. Ramstedt, J.P. Slotte, Membrane properties of sphingomyelins, FEBS Lett. 531 (2002) 33–37.
[51] F.X. Contreras, J. Sot, A. Alonso, F.M. Goni, Sphingosine increases the permeability of model and cell membranes, Biophys. J. 90 (2006) 4085–4092.
[52] F.M. Goni, A. Alonso, Biophysics of sphingolipids I. Membrane properties of sphingosine, ceramides and other simple sphingolipids, Biochim. Biophys. Acta 1758 (2006) 1902–1921.
[53] C. Carrillo, J.A. Teruel, F.J. Aranda, A. Ortiz, Molecular mechanism of membrane permeabilization by the peptide antibiotic surfactin, Biochim. Biophys. Acta 1611 (2003) 91–97.
[54] L. Oftedal, L. Myhren, J. Jokela, G. Gausdal, K. Sivonen, S.O. Doskeland, L. Herfindal, The lipopeptide toxins anabaenolysin A and B target biological membranes in a cholesterol-dependent manner, Biochim. Biophys. Acta 1818 (2012) 3000–3009.
[55] V. Shahedi, G. Oradd, G. Lindblom, Domain-formation in DOPC/SM bilayers studied by pfg-NMR: effect of sterol structure, Biophys. J. 91 (2006) 2501–2507.
[56] M.N. Nasir, F. Besson, Specific interactions of mycosubtilin with cholesterol-containing artificial membranes, Langmuir 27 (2011) 10785–10792.
[57] M. Eeman, G. Francius, Y.F. Dufrene, K. Nott, M. Paquot, M. Deleu, Effect of cholesterol and fatty acids on the molecular interactions of fengycin with Stratum corneum mimicking lipid monolayers, Langmuir 25 (2009) 3029–3039.
[58] M.J. Quentin, F. Besson, F. Peypoux, G. Michel, Action of peptidolipidic antibiotics of the iturin group on erythrocytes. Effect of some lipids on hemolysis, Biochim. Biophys. Acta 684 (1982) 207–211.
[59] J.T. Hannich, K. Umebayashi, H. Riezman, Distribution and functions of sterols and sphingolipids, Cold Spring Harb Perspect Biol 3 (2011) 1.
[60] M. Opekarova, J. Malinsky, W. Tanner, Plants and fungi in the era of heterogeneous plasma membranes, Plant Biol. (Stuttg.) 12 (Suppl. 1) (2010) 94–98.